POLITECNICO DI TORINO
Repository ISTITUZIONALE

Nonlinear dynamics of metamaterial structures based on Kagome lattices using beam finite elements and a component-wise approach

Original
Nonlinear dynamics of metamaterial structures based on Kagome lattices using beam finite elements and a component-wise approach / Augello, R., Carrera, E., Chen, W.Q., Wu, B., Wang, Y.Z.. - In: JOURNAL OF SOUND AND VIBRATION. - ISSN 0022-460X. - 644:(2026). [10.1016/j.jsv.2026.120038]

Availability:
This version is available at: 11583/3017457 since: 2026-11-03T10:56:46Z

Publisher:
Academic Press - Elsevier

Published
DOI:10.1016/j.jsv.2026.120038

Terms of use:

This article is made available under terms and conditions as specified in the corresponding bibliographic description in the repository

Publisher copyright

(Article begins on next page)

21 November 2026

Journal of Sound and Vibration 644 (2026) 120038

Contents lists available at ScienceDirect

Journal of Sound and Vibration

journal homepage: www.elsevier.com/locate/jsvi

Nonlinear dynamics of metamaterial structures based on Kagome lattices using beam finite elements and a component-wise approach

R. Augello [a,1,*], E. Carrera [a,2], W.Q. Chen [b,3], B. Wu [b,4], Y.Z. Wang [b,5]

[a] Mul[2] *Group, Department of Mechanical and Aerospace Engineering, Politecnico di Torino, Corso Duca degli Abruzzi 24, 10129 Torino, Italy*
[b] *Key Laboratory of Soft Machines and Smart Devices of Zhejiang Province, Department of Engineering Mechanics & Soft Matter Research Center, Zhejiang University, 310027 Hangzhou, China*

ARTICLE INFO

Keywords:
Kagome lattice
Metamaterials
Carrera unified formulation
Pre-stressed dynamic analysis
Geometric nonlinearity

ABSTRACT

This paper investigates how external loads and geometric nonlinearities reshape the natural frequencies and mode shapes of a Kagome-lattice mechanical metamaterial. A preload-dependent (pre-stressed) eigenanalysis is performed by linearizing about finite-deformation equilibria obtained using a Carrera Unified Formulation (CUF) of one-dimensional (1D) beam elements enriched by cross-sectional expansion functions. Four configurations are examined: a baseline two-dimensional (2D) lattice, an imperfect lattice with 1.5° pre-rotation, a hinge-stiffened lattice, and a three-dimensional (3D) Kagome architecture. The fundamental mode exhibits softening to buckling followed by hardening; imperfections convert low-order crossings into veering with limited shape change; stiffer hinges flatten frequency-load trends and suppress reshaping. In contrast, the 3D architecture reduces spectral sensitivity and decouples in- and out-of-plane mode families. Higher modes show the largest frequency drops (34.7% in the hinge-stiffened 2D case; 21.9% in 3D). Findings highlight architecture and joint stiffness as primary levers for pre-stress-robust, vibration-resistant designs.

1. Introduction

Metamaterials are engineered materials designed to exhibit extraordinary properties derived mainly from their geometry rather than their composition. This geometric tailoring enables control over a range of physical phenomena [1,2], from wave propagation to stress distribution and energy absorption [3–5]. Such capabilities have made metamaterials indispensable in diverse fields; for example, they have been applied in aerospace and civil structures for vibration isolation, in protective gear for impact energy absorption, and in devices for wave steering and energy harvesting [6–8]. These applications underscore the broad relevance of mechanical

* Corresponding author.
E-mail addresses: riccardo.augello@polito.it (R. Augello), erasmo.carrera@polito.it (E. Carrera), chenwq@zju.edu.cn (W.Q. Chen), bin.wu@zju.edu.cn (B. Wu), yzwangzju@gmail.com (Y.Z. Wang).
[1] Postdoc. E-mail: riccardo.augello@polito.it
[2] Professor of Aeronautics and Astronautics. E-mail: erasmo.carrera@polito.it
[3] Professor. E-mail: chenwq@zju.edu.cn
[4] Tenure-track Professor. E-mail: bin.wu@zju.edu.cn
[5] Researcher. E-mail: yzwangzju@gmail.com

https://doi.org/10.1016/j.jsv.2026.120038
Received 11 March 2026; Received in revised form 29 June 2026; Accepted 30 July 2026
Available online 31 July 2026
0022-460X/© 2026 The Authors. Published by Elsevier Ltd. This is an open access article under the CC BY license (http://creativecommons.org/licenses/by/4.0/).

metamaterials in achieving performance characteristics that surpass those of conventional materials. x Among various metamaterial architectures, the Kagome lattice, a two-dimensional (2D) network of interwoven equilateral triangles, stands out for its unique combination of mechanical and geometric advantages [9]. Originating from a traditional Japanese basket-weaving pattern, the Kagome configuration provides an exceptional balance of high stiffness-to-weight ratio and structural efficiency. Its intrinsic symmetry yields near-isotropic behavior, indicating that it can sustain nearly uniform mechanical responses in all in-plane directions [10,11]. One defining feature of Kagome lattices is their capacity for large deformations without failure, enabled by rigid-body rotations of the triangular units that redistribute loads and dissipate energy [12]. This mechanism makes Kagome lattices ideal for applications requiring high deformability and energy absorption, such as impact mitigation and morphing structures. Indeed, Kagome-based lattices have been used in crashworthy designs to absorb impact energy while maintaining structural integrity. Furthermore, by tailoring their periodic geometry and nodal connections, Kagome metamaterials can achieve exotic effective properties including negative Poisson's ratios [13–15] and tunable stiffness, expanding their potential use in advanced structural systems. These remarkable static and quasi-static characteristics have driven significant interest in Kagome lattices for next-generation aerospace and civil structures that demand lightweight, resilient, and adaptable components.

Beyond their static mechanical behavior, Kagome lattice metamaterials have attracted extensive research attention for controlling wave propagation and dynamic responses [16]. The periodic geometry of a Kagome lattice can be exploited to create phononic band gaps, frequency ranges in which elastic or acoustic waves are attenuated, thereby enabling the filtering or blocking of vibrations at targeted frequencies [17–19]. By adjusting lattice parameters, these band gaps can be tuned, offering a mechanism to selectively inhibit or channel vibrational energy. This functionality has led to the integration of Kagome-based structures in vibration isolation systems and wave-guiding devices, where they serve to attenuate undesirable vibrations or direct wave energy along desired paths. For example, recent works have demonstrated Kagome lattice isolators that suppress low-frequency vibrations in engineering platforms [20,21], as well as waveguiding metastructures that take advantage of the Kagome lattice's symmetry for robust signal transmission [22]. The ability to modulate wave dynamics highlights the versatility of Kagome metamaterials across domains, from mitigating vibrations in aerospace structures to steering acoustic waves in advanced sensor systems. This dynamic wave control is a crucial asset in engineering design, allowing metamaterials not only to bear loads efficiently but also to function as vibration regulators and wave manipulators in smart structures.

Although most of the early studies focused on linear or small-amplitude behavior, there is growing recognition that geometric nonlinearities in metamaterials can unlock entirely new dynamic phenomena and performance gains [23]. Entering the nonlinear regime (e.g., at large deformations or high excitation amplitudes) can break the limitations of linear theory, leading to features such as amplitude-dependent frequency responses, self-adaptive band gaps, and nonreciprocal wave propagation [24]. For example, Deng et al. [25] demonstrated a lattice metamaterial exhibiting an amplitude band gap wherein wave transmission is blocked below a certain excitation amplitude but allowed for larger amplitudes, effectively supporting the formation of elastic solitons in the structure. Such phenomena, which include amplitude-tunable wave attenuation and one-way (nonreciprocal) wave transport, are unattainable in linear metamaterials and point to the immense potential of nonlinear design. In the specific case of Kagome lattices, geometric nonlinearity (stemming from large deflections and rotation of members) can significantly alter their vibrational characteristics. Recent research on flexible Kagome-based metamaterials has revealed the possibility of mode transitions and tunable stiffness under different deformation states [24,26–28]. This means that as a Kagome structure deforms, its natural frequency spectrum and mode shapes can shift; this effect could be harnessed for adaptive vibration control or reconfigurable devices. Moreover, nonlinear vibrations in Kagome lattices may exhibit phenomena such as frequency stiffening or softening, where natural frequencies increase or decrease with vibration amplitude [29]. Under certain conditions, sudden changes in mode shapes, often termed mode jumping, can occur, accompanied by abrupt veering in frequency loci as system parameters vary. These complex behaviors, observed for the first time in Kagome metamaterial panels undergoing large oscillations [30], underscore the importance of studying the nonlinear dynamic regime. A deeper understanding of how geometric nonlinearity influences natural frequencies and mode shapes is crucial for the design of metamaterial structures that remain stable and effective under real operating conditions – conditions that often involve large loads and displacements. It also opens the door to exploiting nonlinearity as a feature, enabling the creation of metamaterials that adapt their vibrational properties in response to external stimuli [31,32].

Quasi-zero stiffness metamaterials are particularly attractive for vibration isolation because they can combine high static load-bearing capacity with low dynamic stiffness around an equilibrium configuration. This feature enables low-frequency vibration isolation without necessarily compromising the ability to sustain external loads. However, their performance is generally restricted to a finite working range and may be sensitive to preload level, geometric imperfections, and stability limits. Negative Poisson's ratio metamaterials, including rotating-unit and re-entrant architectures, are also promising for vibration mitigation because their geometry-induced deformation mechanisms can promote energy absorption, mode coupling, and wave attenuation. On the other hand, these structures may involve complex manufacturing processes, stress concentrations near hinge-like regions, and a strong dependence on loading direction and deformation amplitude. The preload-dependent modal tunability observed in the present Kagome configurations suggests potential applications in adaptive vibration-isolation devices, precision panels, deployable structures, and load-bearing components operating under variable compressive states.

Capturing the aforementioned behaviors in numerical models is nontrivial. Kagome lattices' intricate geometry and deformation mechanisms pose severe challenges for traditional Finite Element Method (FEM) modeling. In a standard FEM approach, accurately resolving the bending and rotation of slender struts and the contact/hinge-like interactions at nodes often demands an extremely fine mesh. For large-scale Kagome structures, this results in prohibitive numbers of elements and degrees of freedom, driving up computational cost and time [33,34]. Conventional 2D or three-dimensional (3D) FEM models may struggle to converge when

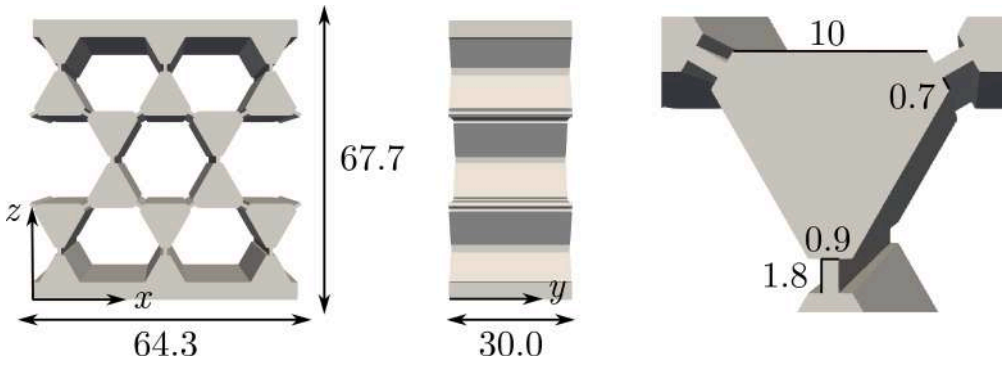


Fig. 1. Considered metamaterial structure based on Kagome mechanism. Geometric characteristics are taken from [16]. Dimensions are expressed in mm.

elements distort under large rotations, and they can miss local phenomena unless the mesh is sufficiently refined around every joint. To address these issues, researchers have explored a spectrum of advanced numerical techniques tailored to lattice metamaterials. One strategy has been enriched finite elements, which incorporate additional kinematic degrees of freedom to capture localized lattice deformation (such as hinge rotations) without uniformly refining the mesh. Another approach is isogeometric analysis, which uses smooth spline-based shape functions to improve accuracy and convergence for complex geometries. IGA has been successfully applied to lattice materials [35–37], offering better representation of curved members and continuum-like behavior in periodic structures. Complementary to these are homogenization methods and reduced-order models [38,39] that simplify the repetitive lattice network into an equivalent continuum or a lower-dimensional model. Such models can drastically cut down computational effort while preserving global stiffness and vibration characteristics, though they may lose detail on local modes. Multi-scale techniques [40–42] have also been proposed, wherein a detailed Kagome unit-cell model is coupled with a coarse global model, allowing localized nonlinear effects to be analyzed without simulating every cell in full detail. Each of these methods can extend the capability of simulations, but each comes with limitations. Often, they rely on simplifying assumptions (e.g., idealized hinge behavior, smeared properties, or truncated basis expansions) that may omit higher-order local phenomena or limit the analysis to small deformation ranges. For instance, a homogenized model might not capture a localized mode in a Kagome hinge, or an enriched element might still assume a planar deformation pattern that cannot represent out-of-plane warping. Furthermore, extending many of these methods to truly 3D Kagome assemblies (as opposed to planar lattices) remains a challenge. Consequently, despite progress in modeling techniques, there is a recognized need for a more direct and high-fidelity modeling framework that can handle the geometric complexity and strong nonlinearities of Kagome metamaterial structures without incurring excessive computational cost [43–45].

In this work, we tackle the modeling challenges by leveraging the Carrera Unified Formulation (CUF) [46,47] in conjunction with the finite element method. CUF provides a powerful framework for developing refined structural models by expanding the kinematic field of an element through additional functions across the cross-section. Specifically, a one-dimensional (1D) beam element can be enriched with a set of expansion functions (such as Lagrange polynomials) that represent the deformation over the cross-section of the element [48]. This approach effectively embeds a higher-order displacement field into the element, allowing it to capture complex deformations (bending, shear, torsion, localized warping, etc.) that standard beam elements or coarse shell models would miss. The ability to include arbitrarily high polynomial orders and custom shape functions makes CUF-based elements particularly well-suited for metamaterial lattices with intricate geometrical features. Unlike conventional FEM, which would require a dense 3D mesh to model each strut and joint, the CUF-enhanced model can represent the Kagome lattice behavior with a handful of 1D elements, significantly reducing model size while maintaining accuracy in capturing both global and local deformations [49,50]. Another key advantage of CUF is its systematic treatment of geometric nonlinearity. The formulation derives the nonlinear governing equations by assembling a consistent tangent stiffness matrix that remains general with respect to the chosen expansion functions. This means large deflections and rotations are handled through an iterative FE solution (e.g., Newton-Raphson or arc-length methods) without the need to fundamentally change the element formulation [51]. This approach has already been validated for the static analysis of Kagome lattices [52]. In this study, the CUF-based finite element framework is extended to the nonlinear dynamic analysis of a Kagome lattice metamaterial, focusing on how external load levels and geometric nonlinearity influence its natural frequencies and mode shapes. By doing so, the limitations of traditional FEM are overcome in this context, and the present work provides new insights into the dynamic tunability and stability of Kagome metamaterial structures. The following sections detail the formulation and demonstrate how the proposed model captures the complex vibration behavior of the Kagome lattice under varying loads, highlighting the critical effects of geometric nonlinearity on its dynamic response.

2. One-dimensional beam finite element for the modeling of metamaterial structures

The Kagome-mechanism metamaterial is shown in Fig. 1; its geometric properties follow [16].
The numerical model is built within the Carrera Unified Formulation (CUF), as outlined in Fig. 2.

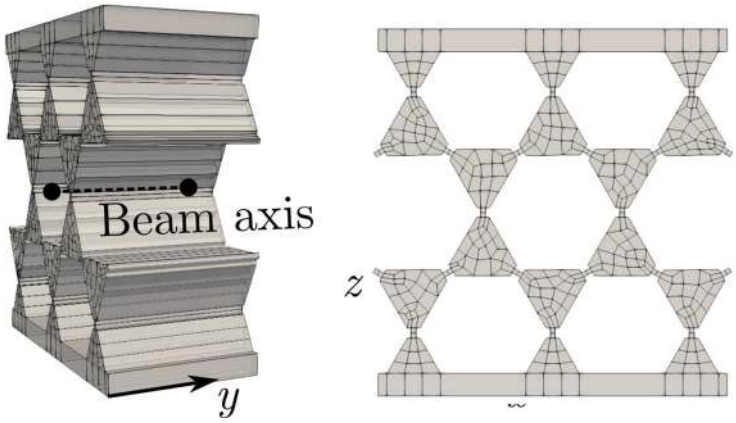


Fig. 2. Carrera unified formulation applied to the metamaterial structure for constructing the mathematical model.

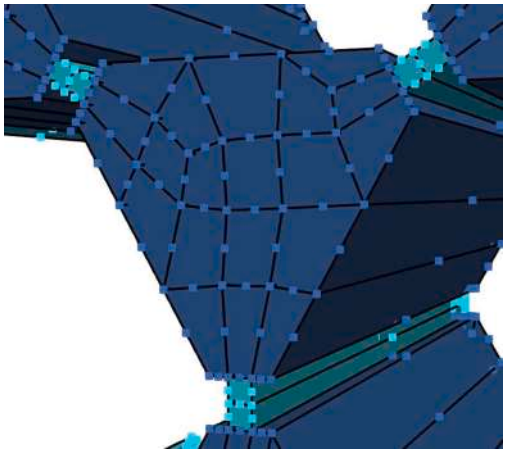


Fig. 3. Connection between rigid triangles and elastic hinges modeled using Lagrange elements.

The 1D model uses x and z as cross-sectional coordinates and y as the axis direction. The 3D displacement field can be written as

$$\mathbf{u}(x,y,z) = \{u_x \quad u_y \quad u_z\}^{\mathrm{T}} \tag{1}$$

where T denotes the transpose operator. Eq. (1) for the 1D metamaterial structure is formulated in CUF and can be expressed as

$$\begin{array}{lcll} \mathbf{u}(x,y,z) & = & F_\tau(x,z)\mathbf{u}_\tau(y), & \tau = 1,2,\ldots,M \\ \delta\mathbf{u}(x,y,z) & = & F_s(x,z)\delta\mathbf{u}_s(y), & s = 1,2,\ldots,M \end{array} \tag{2}$$

ach theory is recovered from Eq. (2) by selecting suitable polynomial orders for F_τ and F_s; in this work, Lagrange polynomials are used. The cross-section is approximated by a pattern of Lagrange Points (LPs) partitioned into appropriate sub-domains. The 3D displacement field results from interpolating the displacements at the LPs, with the interpolation degree set by the number of LPs: 4 (L4) yields a bilinear interpolation, 9 (L9) a quadratic one, and 16 (L16) a cubic one. The total number of DOFs equals the sum of the displacement components at all LPs. For L9, the interpolation functions are

$$\begin{array}{lcll} F_\tau & = & \frac{1}{4}(r^2 + rr_\tau)(s^2 + ss_\tau) & \tau = 1,3,5,7 \\ F_\tau & = & \frac{1}{2}s_\tau^2(s^2 - ss_\tau)(1-r^2) + \frac{1}{2}r_\tau^2(r^2 - rr_\tau)(1-s^2) & \tau = 2,4,6,8 \\ F_\tau & = & (1-r^2)(1-s^2) & \tau = 9 \end{array} \tag{3}$$

with r and s vary from -1 to $+1$, whereas r_τ and s_τ are the natural coordinates of the nine LPs. For more details, see [53] for details. In this study, L9 elements are adopted, and Fig. 3 shows the connection between rigid triangles and elastic hinges modeled with Lagrange elements.

The L9 displacement field is therefore

$$\begin{array}{lcllllll} u_x(x,y,z) & = & F_1(x,z)u_{x_1}(y) & + & F_2(x,z)u_{x_2}(y) & + & \ldots & + & F_9(x,z)u_{x_9}(y) \\ u_y(x,y,z) & = & F_1(x,z)u_{y_1}(y) & + & F_2(x,z)u_{y_2}(y) & + & \ldots & + & F_9(x,z)u_{y_9}(y) \\ u_z(x,y,z) & = & F_1(x,z)u_{z_1}(y) & + & F_2(x,z)u_{z_2}(y) & + & \ldots & + & F_9(x,z)u_{z_9}(y) \end{array} \tag{4}$$

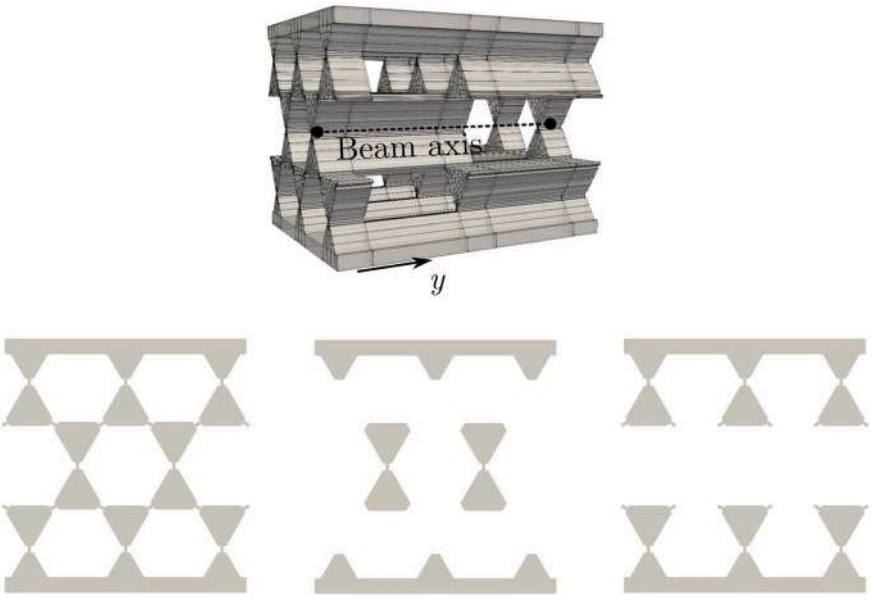


Fig. 4. Using the carrera unified formulation, a mathematical model is constructed for the metamaterial structure by incorporating multiple cross-sectional geometries. The beam cross-sections alternate along the structure's length to capture the overall geometry of the system.

in which $u_{x_1}, \ldots, u_{z_9}$ are the displacement components of each of the nine LPs.

The *generalized* displacements $\mathbf{u}_\tau$ and the *generalized* variations $\delta\mathbf{u}_s$ in Eq. (2) are expanded via the Finite Element Method (FEM) as follows

$$\begin{array}{lcll} \mathbf{u}_\tau(y) & = & N_i(y)\mathbf{q}_{\tau i}, & i = 1, 2, \ldots, N_n \\ \delta\mathbf{u}_s(y) & = & N_j(y)\mathbf{q}_{sj}, & j = 1, 2, \ldots, N_n \end{array} \tag{5}$$

where N_n is the number of the nodes for each Finite Element (FE) and N_i and N_j are the shape functions, $\mathbf{q}_{\tau i}$ and $\mathbf{q}_{sj}$ are the vectors of the FE nodal parameters, expressed as

$$\begin{array}{lcl} \mathbf{q}_{\tau i} & = & \left\{ u_{x_{\tau i}} \; u_{y_{\tau i}} \; u_{z_{\tau i}} \right\}^T \\ \delta\mathbf{q}_{sj} & = & \left\{ \delta u_{x_{sj}} \; \delta u_{y_{sj}} \; \delta u_{z_{sj}} \right\}^T \end{array} \tag{6}$$

The shape functions N_i and N_j are not reported here but can be found in many reference texts, for instance, in Bathe [54]. The explicit forms of the shape functions are standard (see, e.g., Bathe [54]). In this work, the Kagome-based metamaterial is modeled using a single three-node quadratic element (B3).

3. Metamaterial structures with varying cross-section geometry

In the previous example, the goal was to model a Kagome-lattice metamaterial with a cross-section constant along the beam, so deformation was confined to the 2D cross-sectional plane. By contrast, this section examines a metamaterial whose geometry and triangular pattern vary along the axis of the 1D FE model. This variability is achieved via CUF, which allows the cross-sectional geometry to change along the length, enabling the modeling of more complex 3D structures. Fig. 4 depicts the non-uniform cross-section configuration under analysis.

In addition, Fig. 5 reports the dimensions of the three cross-section geometries that alternate to form the full model.

3.1. Geometrical and constitutive relations

The stress, σ, and strain, ϵ, components are written in vector form, without loss of generality,

$$\begin{array}{l} \sigma = \{\sigma_{xx} \;\; \sigma_{yy} \;\; \sigma_{zz} \;\; \sigma_{xz} \;\; \sigma_{yz} \;\; \sigma_{xy}\}^T \\ \epsilon = \{\epsilon_{xx} \;\; \epsilon_{yy} \;\; \epsilon_{zz} \;\; \epsilon_{xz} \;\; \epsilon_{yz} \;\; \epsilon_{xy}\}^T \end{array} \tag{7}$$

For the kinematics, the Green-Lagrange nonlinear strain components are

$$\boldsymbol{\epsilon} = \boldsymbol{\epsilon}_l + \boldsymbol{\epsilon}_{nl} = (\mathbf{b}_l + \mathbf{b}_{nl})\mathbf{u}, \tag{8}$$

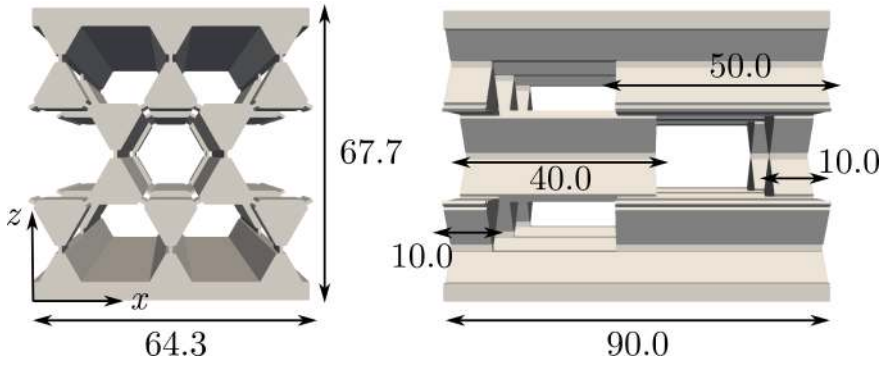


Fig. 5. Geometric properties of the metamaterial structure with different cross-sections. The dimensions are expressed in mm. The dimensions not shown are the same as those in Fig. 1.

The 6×3 linear and nonlinear differential operators $\mathbf{b}_l$ and $\mathbf{b}_{nl}$ in Eq. (8) are

$$\mathbf{b}_l = \begin{bmatrix} \partial_x & 0 & 0 \\ 0 & \partial_y & 0 \\ 0 & 0 & \partial_z \\ \partial_z & 0 & \partial_x \\ 0 & \partial_z & \partial_y \\ \partial_y & \partial_x & 0 \end{bmatrix}, \qquad \mathbf{b}_{nl} = \begin{bmatrix} \frac{1}{2}(\partial_x)^2 & \frac{1}{2}(\partial_x)^2 & \frac{1}{2}(\partial_x)^2 \\ \frac{1}{2}(\partial_y)^2 & \frac{1}{2}(\partial_y)^2 & \frac{1}{2}(\partial_y)^2 \\ \frac{1}{2}(\partial_z)^2 & \frac{1}{2}(\partial_z)^2 & \frac{1}{2}(\partial_z)^2 \\ \partial_x\partial_z & \partial_x\partial_z & \partial_x\partial_z \\ \partial_y\partial_z & \partial_y\partial_z & \partial_y\partial_z \\ \partial_x\partial_y & \partial_x\partial_y & \partial_x\partial_y \end{bmatrix} \tag{9}$$

where $\partial_\alpha = \partial(\cdot)/\partial\alpha$, $\partial_\beta = \partial(\cdot)/\partial\beta$, and $\partial_z = \partial(\cdot)/\partial z$. For the constitutive law, linear-elastic metallic shell structures are considered. The relation is

$$\boldsymbol{\sigma} = \mathbf{C}\boldsymbol{\epsilon} \tag{10}$$

where $\mathbf{C}$ is the elastic material matrix; its explicit form is standard (see [54,55]). Finally, introducing the CUF and FEM relations into Eq. (8), the strain vector can be written in algebraic form as

$$\boldsymbol{\epsilon} = (\mathbf{B}_l^{\tau i} + \mathbf{B}_{nl}^{\tau i})\mathbf{q}_{\tau i} \tag{11}$$

where $\mathbf{B}_l^{sj}$ and $\mathbf{B}_{nl}^{sj}$ denote the linear and nonlinear algebraic matrices within CUF and FEM formulations. Their explicit expressions are omitted for brevity; see [56].

4. Nonlinear free vibration

This section outlines the formulation for vibration analysis. The principle of virtual displacements is recalled: the virtual variation of internal strain energy and inertial forces equals the virtual variation of external forces. The virtual variation of strain energy is used to define the secant stiffness matrix $\mathbf{K}_S$, namely:

$$\begin{aligned} \delta L_{\text{int}} &= \delta\mathbf{q}_{sj}^T \int_\Omega (\mathbf{B}_l^{sj} + 2\mathbf{B}_{nl}^{sj})^T \boldsymbol{\sigma}\, \mathrm{dV} = \\ &= \delta\mathbf{q}_{sj}^T \int_\Omega (\mathbf{B}_l^{sj} + 2\mathbf{B}_{nl}^{sj})^T \mathbf{C}(\mathbf{B}_l^{\tau i} + \mathbf{B}_{nl}^{\tau i})\, \mathrm{dV}\mathbf{q}_{\tau i} = \\ &= \delta\mathbf{q}_{sj}^T \mathbf{K}_0^{ij\tau s}\mathbf{q}_{\tau i} + \delta\mathbf{q}_{sj}^T \mathbf{K}_{lnl}^{ij\tau s}\mathbf{q}_{\tau i} \\ &+ \delta\mathbf{q}_{sj}^T \mathbf{K}_{nll}^{ij\tau s}\mathbf{q}_{\tau i} + \delta\mathbf{q}_{sj}^T \mathbf{K}_{nlnl}^{ij\tau s}\mathbf{q}_{\tau i} \\ &= \delta\mathbf{q}_{sj}^T \mathbf{K}_S^{ij\tau s}\mathbf{q}_{\tau i} \end{aligned} \tag{12}$$

Here, $\mathbf{K}_0^{ij\tau s}$ denotes the linear part of $\mathbf{K}_S$, while $\mathbf{K}_{lnl}^{ij\tau s}$, $\mathbf{K}_{nll}^{ij\tau s}$, and $\mathbf{K}_{nlnl}^{ij\tau s}$ collect the nonlinear contributions. These components are expressed as CUF 3×3 Fundamental Nuclei (FNs), which serve as the elemental building blocks of the theory. Each FN is independent of the specific theory order and is expanded via the F_τ approximation ($\tau, s = 1, \ldots, M$) and the shape functions N_i ($i, j = 1, \ldots, N_n$), yielding the stiffness matrix of any high-order model. The global matrix $\mathbf{K}_S$ follows by looping over these indices. Applying the principle of virtual work–omitting the external virtual work for brevity–leads to the system of nonlinear equilibrium equations:

$$\mathbf{K}_S^{ij\tau s}\, \mathbf{q}_{\tau i} = \mathbf{p}_{sj} \tag{13}$$

In Eq. (13), $\mathbf{p}_{sj}$ denotes the FNs of the secant stiffness matrix and the nodal load vector. The solution is obtained with the Newton-Raphson method coupled with an arc-length strategy [57,58]. In an analogous way, the FNs of the mass matrix follow from the virtual variation of inertial loads:

$$\delta L_{\text{int}} = \delta\mathbf{q}_{sj}^T \mathbf{M}^{ij\tau s}\ddot{\mathbf{q}}_{\tau i} \tag{14}$$

where $\mathbf{M}^{ij\tau s}$ is the FN of the mass matrix and $\ddot{\mathbf{q}}_{\tau i}$ the nodal accelerations (dot = time derivative). Since modal behavior depends on the equilibrium state, eigenfrequencies and eigenmodes may undergo sudden changes in deep nonlinear regimes [59]. To assess this, vibration analysis is carried out about linearized equilibria along the nonlinear path. Linearizing the virtual variation of the nonlinear strain energy introduces the tangent stiffness $\mathbf{K}_T$:

$$\begin{aligned} &\delta(\delta L_{\text{int}} + \delta L_{\text{ine}} - \delta L_{\text{ext}}) \\ &\delta\mathbf{q}_{sj}^T(\mathbf{K}_0^{ij\tau s} + \mathbf{K}_{T1}^{ij\tau s})\mathbf{q}_{\tau i} + \delta\mathbf{q}_{sj}^T\mathbf{K}_\sigma^{ij\tau s}\mathbf{q}_{\tau i} + \delta\mathbf{q}_{sj}^T\mathbf{M}^{ij\tau s}\ddot{\mathbf{q}}_{\tau i} \\ &\delta\mathbf{q}_{sj}^T\mathbf{K}_T^{ij\tau s}\mathbf{q}_{\tau i} + \delta\mathbf{q}_{sj}^T\mathbf{M}^{ij\tau s}\ddot{\mathbf{q}}_{\tau i} = 0 \end{aligned} \tag{15}$$

In deriving Eq. (15), the mass matrix is taken as linear and $\delta^2 L_{\text{ext}} = 0$ (conservative loading). Here, $\mathbf{K}_T^{ij\tau s}$ is the FN of the tangent stiffness matrix; $\mathbf{K}_0^{ij\tau s}$ is its linear part; $\mathbf{K}_{T1}^{ij\tau s} = 2\mathbf{K}_{lnl}^{ij\tau s} + \mathbf{K}_{nll}^{ij\tau s} + 2\mathbf{K}_{nlnl}^{ij\tau s}$ is the nonlinear contribution; and $\mathbf{K}_\sigma^{ij\tau s}$ is the geometric stiffness, which depends on the linear ($\mathbf{K}_\sigma{}^{ij\tau s}$) and nonlinear ($\mathbf{K}_{\sigma_{nl}}^{ij\tau s}$) pre-stress state, with

$$\sigma = \sigma_l + \sigma_{nl} = \mathbf{C}(\epsilon_l + \epsilon_{nl}) \tag{16}$$

The full global stiffness matrices are obtained by assembling the FNs over $\tau, s = 1, \dots, M$ and $i, j = 1, \dots, p+1$. For details on FN expansion and FE assembly within CUF, see Carrera et al. [47].

Small displacement variations are assumed in Eq. (15), allowing harmonic motion and hence a linear eigenvalue formulation around nonlinear equilibria. The workflow is as follows:

- Solve the static geometrically nonlinear problem with Newton-Raphson and arc-length control.
- Along the resulting equilibrium path, compute the tangent stiffness at each state of interest.
- Then, considering the incremental linearized equilibrium of Eq. (15) and assuming harmonic motion around nontrivial equilibria,

$$\begin{aligned} \delta\mathbf{q}_{\tau i}(t) &= \delta\tilde{\mathbf{q}}_{\tau i}e^{i\omega t} \\ \delta\ddot{\mathbf{q}}_{\tau i}(t) &= -\omega^2\delta\tilde{\mathbf{q}}_{\tau i}e^{i\omega t} \end{aligned} \tag{17}$$

  the equations of motion reduce to a linear eigenproblem for natural frequencies and mode shapes:

$$(\mathbf{K}_T^{ij\tau s} - \omega^2\mathbf{M}^{ij\tau s})\tilde{\mathbf{q}}_{\tau i}e^{i\omega t} = 0 \tag{18}$$

  Here, ω is the natural frequency and $\tilde{\mathbf{q}}_{\tau i}$ the eigenvector. It is also emphasized that nonlinear vibrations are of small amplitude, and only small increments are considered, which justifies linearization about the equilibrium state.

A linearized resolution is standard in much of the literature; therefore, this work contrasts linear and nonlinear approaches to show when a full nonlinear formulation is required for accuracy. Linearizing about the trivial equilibrium yields

$$\mathbf{K}_T = \mathbf{K}_0 + \lambda\mathbf{K}_{\sigma l} \tag{19}$$

where λ is the monotonically increasing load factor. This simplified approach follows by substituting Eq. (19) into Eq. (15), where $\mathbf{K}_{T1}$ vanishes due to the smallness of δu.

5. Numerical results

The numerical campaign investigates mode switching phenomena and the evolution of the associated natural frequencies of a Kagome-lattice metamaterial subjected to increasing uniaxial compression. The study cases follow [52], which reports the geometrically nonlinear static responses of the same structures. From those paths, a set of representative equilibrium configurations is sampled; at each configuration, the pre-stressed small-amplitude dynamics is obtained by linearizing about the equilibrium and solving the generalized eigenproblem. Modes are tracked along the path to detect crossings/veerings, mode reshaping, and reordering. The cases considered are:

- **Baseline Kagome metastructure under compression.** Evolution of the first 10 frequencies and shapes from the pre-buckling regime into post-buckling branches, highlighting symmetry breaking, frequency drops, and veering events.
- **Sensitivity to (i) initial conditions and (ii) hinge stiffness.** Quantifies how (i) initian conditions and (ii) stiffer hinge modeling shift critical loads, alter mode ordering, and modify frequency-load slopes; implications for robustness and design margins are discussed.
- **3D Kagome metastructure.** Extension to a 3D Kagome variant to assess different effects and potential band gap opening/closure under compressive pre-stress, with direct comparison to the 2D baseline.

Across all cases, results are presented through frequency-load diagrams and the associated mode shape evolution, providing a clear identification of mode-switching points and the associated dynamic consequences. In the following discussion, the terms mode veering, mode crossing, and mode reshaping are used according to the combined observation of frequency-load curves and mode-shape evolution. Mode veering is identified when two frequency branches approach each other and then separate without a clear intersection, together with a visible interaction between the corresponding deformation patterns. Mode crossing is associated with branches that intersect, or nearly intersect, without a relevant qualitative change in their modal shapes. Mode reshaping denotes a significant modification of the spatial deformation pattern of a mode along the nonlinear equilibrium path, even when the associated frequency does not change substantially. Since the accuracy of the present CUF-based component-wise beam model for Kagome lattice metamaterials has already been assessed in [52], the numerical validation of the structural discretization is not repeated here. Accordingly, the validated modeling framework is adopted in the following geometrically nonlinear dynamic analyses.

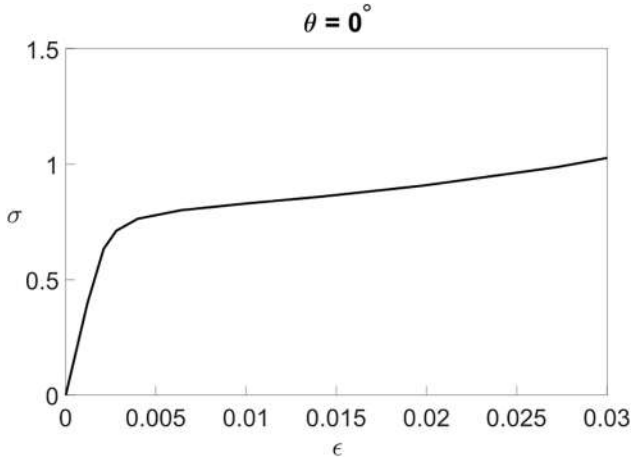


Fig. 6. σ vs. ϵ evolution for the metamaterial Kagome structure. σ is calculated as the applied force F divided by the area over which the force is applied. ϵ is determined as the ratio of the vertical displacement of the top plate to the initial height of the structure, which is 67.60 mm.

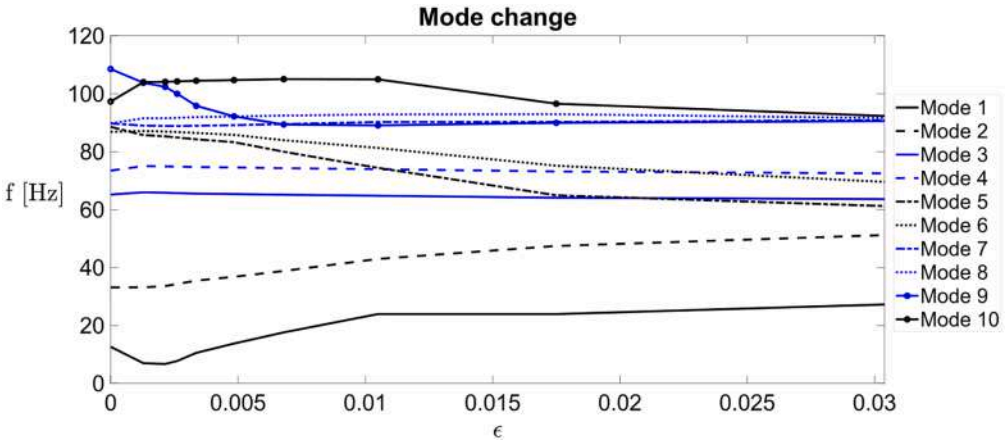


Fig. 7. Evolution of the first 10 natural frequencies of the metamaterial Kagome structure.

5.1. Kagome mechanism

The first analysis concerns the Kagome metastructure shown in Fig. 1. The specimen is subjected to a uniform transverse compression applied on the top surface, while the bottom surface is clamped. The finite-element model comprises 30,600 degrees of freedom. Isotropic properties are assumed for the components. The stiff triangular domains are modeled with Young's modulus E = 2.35 GPa and Poisson's ratio $\nu = 0.375$; the soft hinges are assigned E = 0.14 GPa and $\nu = 0.480$. The static equilibrium path is reported in Fig. 6.

The evolution of the first ten natural frequencies along the same sequence of equilibria is shown in Fig. 7, and the numerical values are listed in Table 1.

Several observations follow: **Mode 1** (in-plane). The frequency decreases as the load increases, up to the onset of buckling; beyond that point, it rises again, indicating post-buckling stiffness recovery driven by the changed tangent operator. This qualitative softening-hardening trend is consistent with the literature on pre-stressed lattices and post-buckling dynamics [60]. The corresponding mode-shape evolution is illustrated in Fig. 8 (left) for $\epsilon = 0.00$ and $\epsilon = 2.86$, clearly showing the change.

Mode 2 (first out-of-plane). The associated shape evolves with load (see Fig. 8, right), though less markedly than Mode 1. Its frequency remains comparatively insensitive to the buckling event and exhibits only mild variation across the path, indicating limited coupling with the primary in-plane instability.

Mode 3. Along the entire equilibrium path the frequency remains nearly constant, whereas the mode shape changes significantly (Fig. 9, left). This points to a shape reshaping without appreciable spectral drift, a behavior often associated with weak veering with neighboring modes.

Mode 5. This mode experiences the largest spectral change, with the frequency decreasing from 88.57 Hz to 59.18 Hz. Interestingly, the corresponding shape remains essentially unchanged (Fig. 9, right), suggesting that the observed drop is primarily due to

Table 1
Natural frequency values of the metamaterial Kagome structure.

	Mode frequency									
ϵ	1	2	3	4	5	6	7	8	9	10
0.00	12.64	33.15	65.20	73.46	88.57	86.86	89.74	89.76	97.32	108.52
0.08	6.97	33.17	65.96	75.02	85.71	87.14	88.99	91.52	103.78	104.00
0.14	6.71	33.60	65.82	74.93	85.29	86.94	88.88	91.55	102.37	104.10
0.17	7.75	34.33	65.68	74.83	84.90	86.76	88.85	91.68	99.97	104.25
0.22	10.54	35.49	65.52	74.69	84.26	86.45	88.95	91.92	95.83	104.47
0.46	17.61	38.82	65.14	74.29	79.97	83.95	89.51	92.45	89.39	105.05
1.18	23.93	47.45	64.10	73.16	64.93	75.14	90.26	92.94	89.94	96.55
2.06	27.26	51.23	63.62	72.50	61.19	69.53	90.86	91.60	90.55	92.29
2.86	30.33	53.33	63.04	71.89	59.18	64.97	89.84	91.13	88.05	91.61

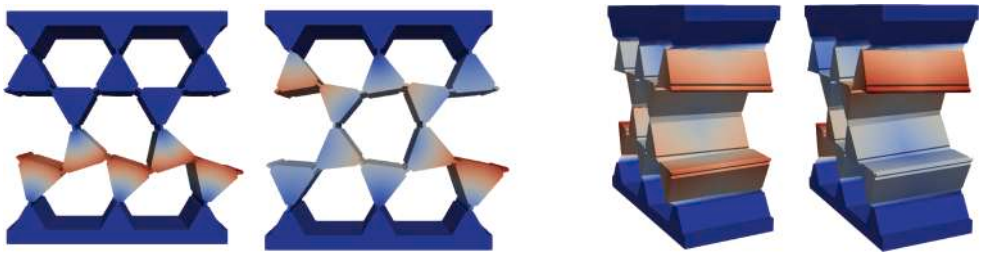


Fig. 8. First and second mode shapes of the metamaterial Kagome structure.

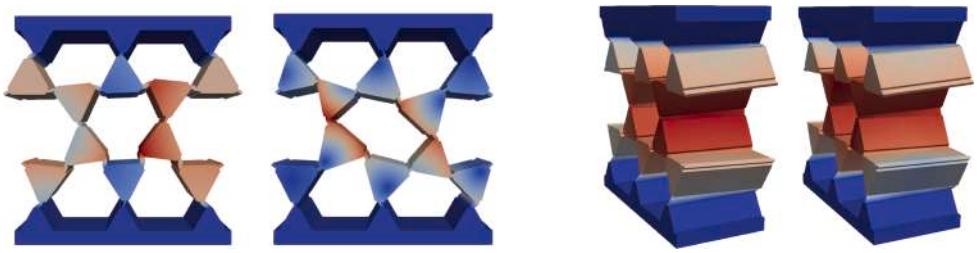


Fig. 9. Third and fifth mode shapes of the metamaterial Kagome structure.

stress-stiffening relief in the same deformation pattern rather than a mode exchange. In other words, no identity swap is evident for Mode 10 despite its strong frequency sensitivity.

Overall, the results highlight three recurring mechanisms in compressed Kagome lattices: (i) a fundamental softening up to buckling followed by post-buckling hardening; (ii) out-of-plane modes that reshape with load yet remain spectrally stable; and (iii) higher-order modes with strong frequency sensitivity but nearly invariant shapes.

5.1.1. Influence of initial conditions

The second case assesses the influence of initial conditions on the dynamic response. Before loading, all rigid triangular units are pre-rotated by 1.5° relative to the reference configuration. The 1.5° pre-rotation is imposed on the rigid triangular units in the initial, unloaded configuration. It is introduced as a deterministic geometric imperfection, or equivalently as a controlled structural bias, in order to break the symmetry of the ideal Kagome mechanism and to select a preferred deformation path under compression. From a practical viewpoint, this small pre-rotation can be interpreted as representative of manufacturing or assembly imperfections. From a numerical viewpoint, it allows the sensitivity of the preload-dependent modal response to small deviations from the perfect geometry to be assessed. The metastructure is then subjected to the same uniform transverse pressure as in the baseline analysis. The corresponding static equilibrium curve is shown in Fig. 10.

The evolution of the first ten natural frequencies along that path is reported in Fig. 11, with numerical values in Table 2. Mode tracking is performed as in the previous section to ensure consistent identification across equilibria. Some local irregularities can be observed in the frequency-load curves, especially in regions where two or more modes become close in frequency. These points should not be interpreted as a loss of convergence of the nonlinear static solution. They are mainly related to the strong modal interaction that occurs in the pre-stressed configuration and to the rapid variation of the tangent stiffness along the nonlinear equilibrium path. Since the eigenvalue problem is solved independently at each sampled equilibrium state, the ordering of close modes may change locally from one load level to the next. As a consequence, small apparent jumps or scattered points may appear in the frequency evolution. These features are therefore interpreted as indicators of mode interaction, stress-stiffening or stress-softening redistribution, and load-dependent changes in the tangent stiffness of the Kagome lattice.

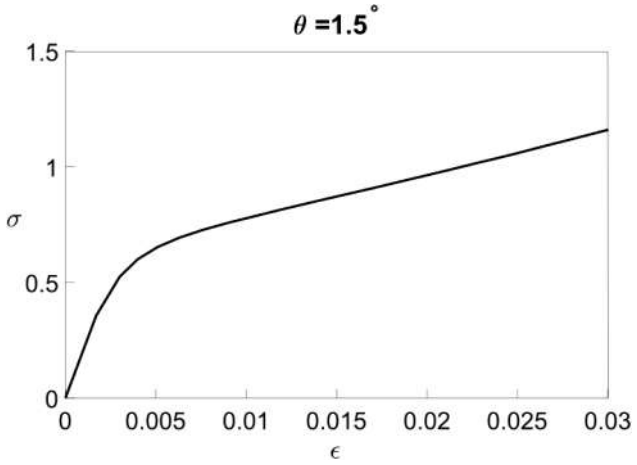


Fig. 10. σ vs. ϵ evolution for the metamaterial Kagome structure with initial conditions. σ is calculated as the applied force F divided by the area over which the force is applied. ϵ is determined as the ratio of the vertical displacement of the top plate to the initial height of the structure, which is 67.60 mm.

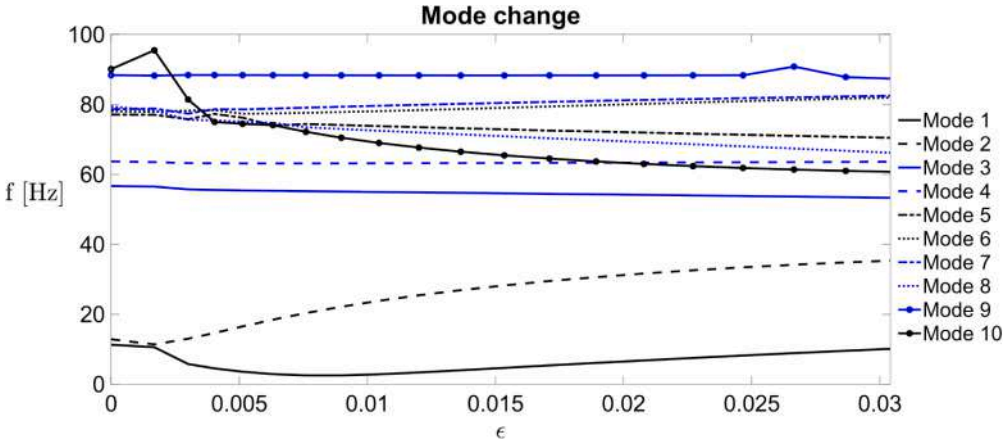


Fig. 11. Evolution of the first 10 natural frequencies of the metamaterial Kagome structure with initial conditions.

Table 2
Natural frequency values of the metamaterial Kagome structure with initial conditions.

	Mode frequency									
ϵ	1	2	3	4	5	6	7	8	9	10
0.00	11.26	12.82	56.66	63.67	77.08	78.02	78.61	79.41	88.35	90.08
0.27	4.50	14.63	55.52	63.16	77.27	78.37	78.62	75.38	88.38	74.97
0.51	2.50	20.32	55.16	63.13	74.40	77.58	79.05	73.45	88.32	72.15
0.70	2.82	23.83	54.94	63.16	73.78	78.06	79.59	72.46	88.29	68.96
1.03	4.65	28.22	54.57	63.25	72.85	79.02	80.44	70.89	88.27	65.42
1.53	7.49	32.56	53.97	63.40	71.62	80.54	81.52	68.61	88.30	62.34
1.66	8.18	33.39	53.80	63.45	71.31	80.92	81.78	68.00	88.32	61.81
1.80	8.87	34.14	53.62	63.49	71.00	81.30	82.02	67.37	90.81	61.35
2.07	10.19	35.38	53.26	63.59	70.39	81.96	82.49	66.05	87.28	60.67

Compared with the baseline, the imperfection shifts the apparent buckling threshold and regularizes the spectrum in the low-order range. In particular, a pronounced veering between Modes 1 and 2 emerges near the buckling-like transition. However, unlike the baseline case where Mode 1 exhibited marked reshaping across the instability the present configuration shows minimal shape changes for both modes.

This is evident in Fig. 12 (left/right), which depicts Modes 1 and 2 at $\epsilon = 0.00$ and $\epsilon = 2.07$: the geometries remain qualitatively similar despite the spectral repulsion. The interpretation is that the 1.5° pre-rotation breaks symmetry and biases the stress field, so the subsequent loss of stability perturbs the tangent stiffness less dramatically in the modal subspace spanned by Modes 1-2; the result is strong frequency interaction with limited geometric reshaping.

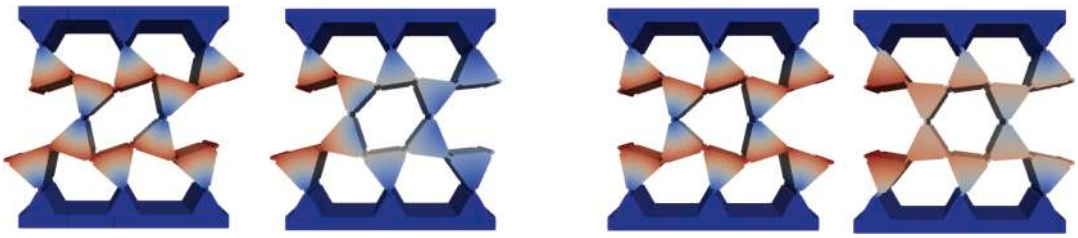


Fig. 12. First and second mode shapes of the metamaterial Kagome structure with initial conditions.

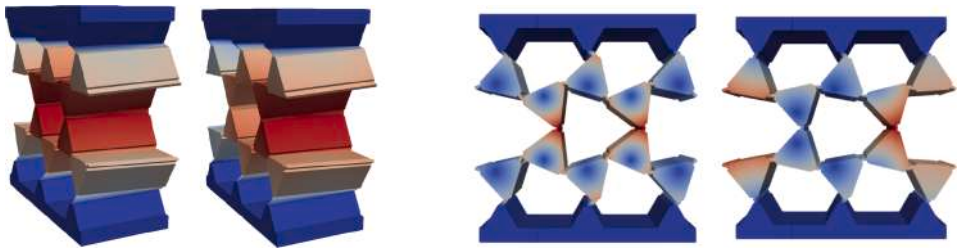


Fig. 13. Third and tenth mode shapes of the metamaterial Kagome structure with initial conditions.

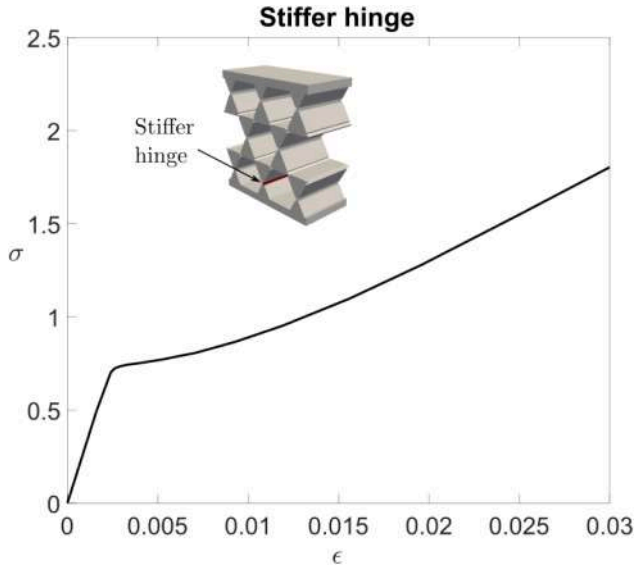


Fig. 14. σ vs. ϵ evolution for the metamaterial Kagome structure with stiffer hinge. σ is calculated as the applied force F divided by the area over which the force is applied. ϵ is determined as the ratio of the vertical displacement of the top plate to the initial height of the structure, which is 67.60 mm.

Mode 3 (first out-of-plane) remains spectrally and geometrically stable along the path in this imperfection scenario: both frequency drift and shape changes are small (cf. Fig. 13, left for the out-of-plane), indicating weak coupling between the dominant in-plane pre-stress and out-of-plane DOFs when the lattice is pre-rotated. This contrasts with the baseline, where Mode 3 displayed noticeable shape evolution at nearly constant frequency. At higher order, Mode 10 exhibits the largest spectral sensitivity, with its frequency decreasing from 90.08 Hz to 60.67 Hz, while its shape remains essentially invariant. This mirrors the mechanism observed previously for high-order modes: the frequency drop is primarily governed by stress-stiffening relief in the same deformation pattern, rather than by a mode shape exchange.

Taken together, these results demonstrate that small, realistic assembly imperfections can (a) attenuate modal reshaping near the first instability, (b) convert sharp crossings into avoided crossings (veering) for the lowest modes, and (c) leave out-of-plane largely decoupled, even as higher modes undergo significant frequency degradation with nearly frozen shapes.

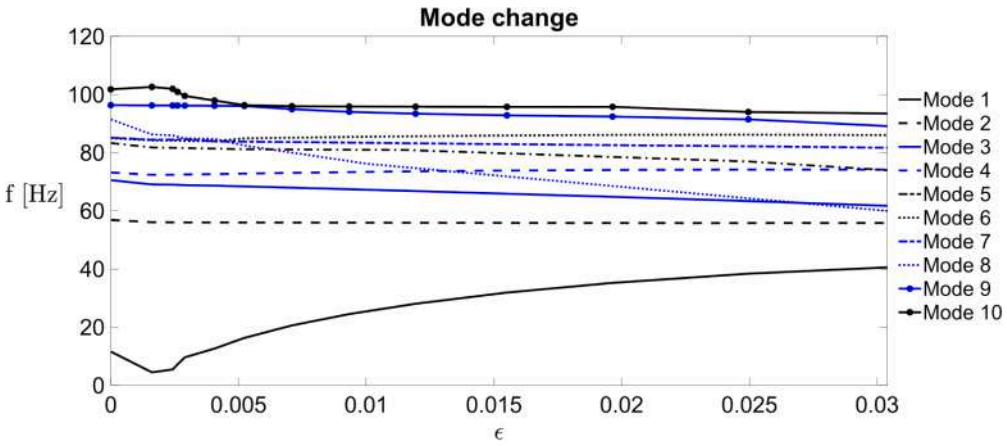


Fig. 15. Evolution of the first 10 natural frequencies of the metamaterial Kagome structure with stiffer hinge.

Table 3
Natural frequency values of the metamaterial Kagome structure with stiffer hinges.

	Mode frequency									
ϵ	1	2	3	4	5	6	7	8	9	10
0.00	11.63	56.89	70.56	73.20	83.34	85.05	85.17	91.48	96.35	101.81
0.18	7.23	56.08	68.96	72.45	81.72	84.13	84.56	85.55	96.23	100.93
0.35	16.33	56.03	68.41	72.82	81.21	84.94	83.84	82.49	96.07	96.35
0.63	24.54	55.97	67.45	73.35	81.30	85.43	83.46	76.90	94.06	95.90
0.81	28.08	55.93	66.82	73.60	80.88	85.67	83.24	74.31	93.42	95.83
1.05	31.93	55.88	65.89	73.87	80.13	85.94	82.94	71.04	92.85	95.78
1.69	38.43	55.84	63.37	74.21	76.99	86.21	82.22	63.65	91.47	94.00
2.08	40.71	55.86	61.65	74.20	73.83	86.04	81.70	59.78	89.02	93.46

Table 4
Natural frequency values of the 3D metamaterial Kagome structure.

	Mode frequency									
ϵ	1	2	3	4	5	6	7	8	9	10
0.00	8.47	9.60	34.62	48.56	49.84	58.85	58.53	57.89	57.90	64.24
0.03	7.63	8.96	34.38	48.41	49.60	57.60	57.75	57.99	58.73	64.21
0.09	5.56	7.57	33.90	48.11	49.11	56.72	57.13	57.45	58.48	64.13
0.13	3.95	6.85	33.64	47.93	48.83	56.06	56.79	57.26	58.34	64.08
0.29	2.86	10.05	33.45	47.54	48.06	54.50	56.49	56.66	58.01	63.91
0.44	3.29	13.85	33.74	47.61	47.39	53.84	56.85	56.13	57.86	61.87
0.72	1.66	19.15	34.42	47.15	46.83	52.72	57.65	54.67	57.72	59.18
1.09	3.75	23.47	35.23	46.84	45.97	51.39	58.16	52.72	58.83	57.45
1.50	6.00	26.62	36.05	46.47	45.09	50.00	57.73	51.12	59.98	57.22
1.96	10.01	29.06	37.12	46.03	44.35	48.60	57.56	50.22	61.18	56.99
2.42	11.28	30.17	37.89	45.48	43.18	47.11	57.42	49.53	61.93	56.52
2.94	12.94	30.70	38.67	44.91	42.00	45.94	57.34	49.40	61.36	55.80

5.1.2. Influence of stiffer hinge

The third case evaluates the effect of stiffer hinges while preserving the loading scenario of the baseline (uniform transverse pressure; clamped base). The corresponding static equilibrium curve is shown in Fig. 14. As in the previous sections, the pre-stressed small-amplitude dynamics is obtained by linearizing about sampled equilibrium states and solving the generalized eigenproblem.

The evolution of the first ten natural frequencies is reported in Fig. 15, with numerical values in Table 3. Similar considerations apply to the local irregularities observed in Fig. 15, where close frequency branches and the load-dependent tangent stiffness lead to local changes in modal ordering.

The first frequency exhibits the familiar softening-hardening trend around the buckling-like transition: it decreases up to the instability and then increases afterwards, reflecting the change in the tangent stiffness operator in post-buckling. Unlike the baseline configuration, the mode shape varies only marginally across equilibria (see Fig. 16), indicating that hinge stiffening suppresses the symmetry-breaking features that previously drove stronger reshaping. Modes 2 and 5 remain spectrally steady and geometrically consistent. Figs. 16-17 show that the second mode is essentially invariant, while the fifth mode displays only a slight redistribution of curvature (minor reshaping) with negligible frequency drift.

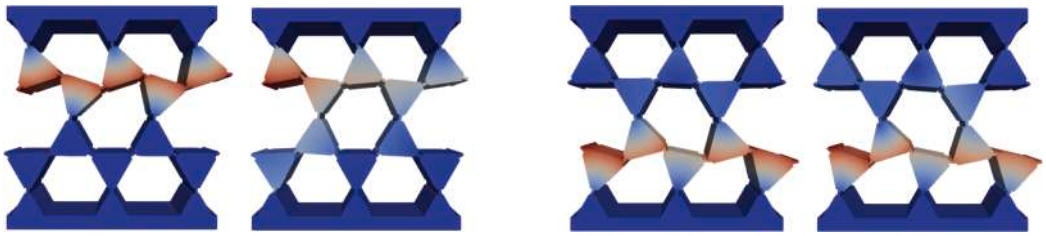


Fig. 16. First and second mode shapes of the metamaterial Kagome structure with stiffer hinge.

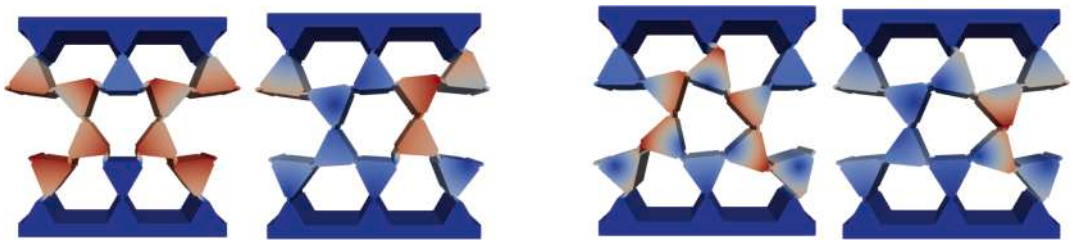


Fig. 17. Fifth and eighth mode shapes of the metamaterial Kagome structure with stiffer hinge.

Mode 8 retains the largest frequency variation, decreasing from 91.48 Hz to 59.78 Hz, a 34.7% reduction, closely matching the percentage drop observed in the imperfection study (about 32.6% for Mode 10 there). Despite this spectral sensitivity, the mode shape remains practically unchanged across the equilibrium path (Fig. 17), indicating a stress-stiffening relief within the same deformation pattern rather than a mode identity exchange. Hinge stiffening increases the local rotational constraints at joints, which raises the effective tangent stiffness seen by low-order in-plane mechanisms and damps the coupling that leads to veering and strong reshaping. Consequently, low- and mid-order modes are shape-stable, while selected higher modes can still show sizeable frequency drops driven by pre-stress effects without altering their identity.

5.2. *Three-dimensional Kagome mechanism*

The fourth case examines the mode evolution of a 3D Kagome metamaterial (see Figs. 4 and 5). The boundary and loading conditions are identical to the earlier studies (uniform transverse pressure; clamped base). The static equilibrium curve is shown in Fig. 18; the evolution of the first ten natural frequencies along that path is reported in Fig. 19 and summarized numerically in Table 4. As before, pre-stressed small-amplitude dynamics is obtained by linearizing about sampled equilibria and solving the generalized eigenproblem,

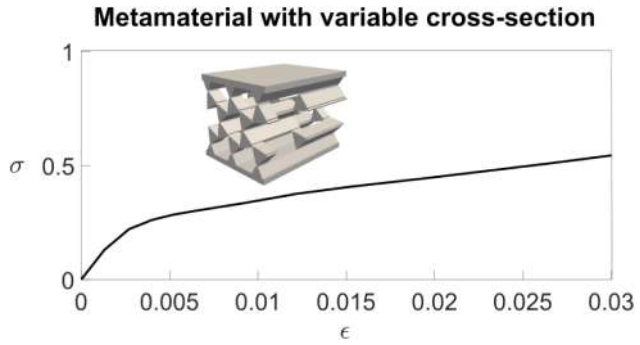


Fig. 18. σ vs. ϵ evolution for the 3D metamaterial Kagome structure. σ is calculated as the applied force F divided by the area over which the force is applied. ϵ is determined as the ratio of the vertical displacement of the top plate to the initial height of the structure, which is 67.60 mm.

A clear veering between Modes 1-2 appears near the transition region, akin to the imperfection case, but without a pronounced low-order softening. (ii) Across the first ten modes, no large monotonic decreases are observed in the low order; the largest spectral drop is 21.9% and occurs for Mode 6, notably smaller than 34.7% maximum seen previously (hinge-stiffened case). Most higher modes remain remarkably flat compared with the 2D counterparts.

Both in-plane families (Fig. 20) and out-of-plane families (Fig. 21) exhibit nearly invariant shapes along the equilibrium path; any differences are limited to minor. In particular, the first two modes–despite the veering–retain their geometric identity with only

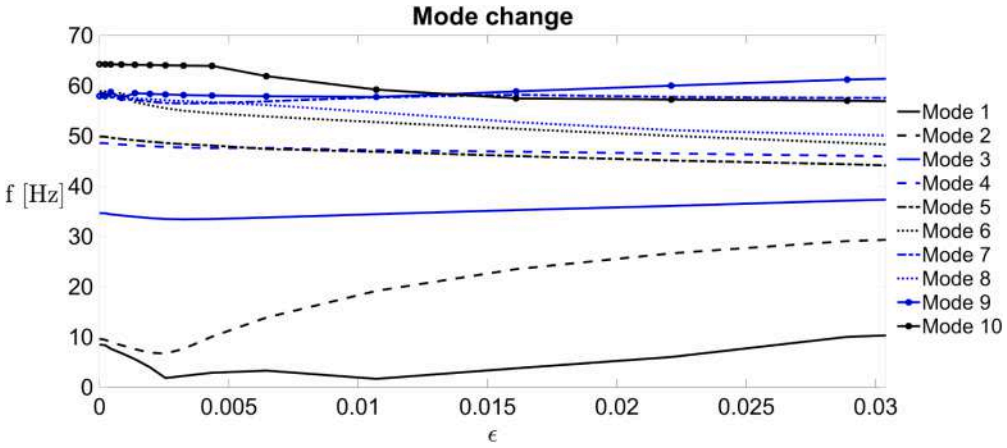


Fig. 19. Evolution of the first 10 natural frequencies of the 3D metamaterial Kagome structure.

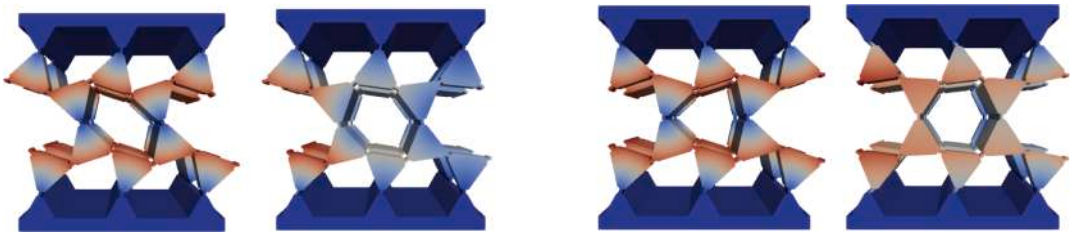


Fig. 20. First and second mode shapes of the 3D metamaterial Kagome structure.

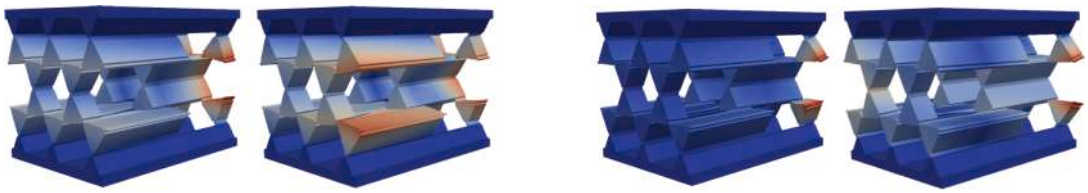


Fig. 21. Third and tenth mode shapes of the 3D metamaterial Kagome structure.

subtle reshaping, while mid- and high-order modes remain effectively unchanged even where frequency shifts occur (e.g., Mode 6). The added connections of the 3D architecture increases torsional and bending constraints and raises the effective tangent stiffness seen by the dominant mechanisms. This suppresses the geometric-nonlinear coupling that, in the 2D cases, drove stronger reshaping and larger stress-stiffening relief. Consequently low-order modes show avoided crossings without major softening or identity swaps. Mid/high-order modes experience smaller spectral drift and both in-plane and out-of-plane families are more decoupled, which explains the flat, stable frequency-load trends for most higher modes.

Because mode shapes remain essentially constant while frequencies vary modestly, the 3D Kagome exhibits robust modal identity under pre-stress. This has several practical payoffs, including predictable control and monitoring. Reduced mode mixing/reshaping simplifies controller tuning and health-monitoring models linearized about changing equilibria.

6. Conclusions

This work investigated the dynamic response of Kagome-lattice metastructures, in terms mode and frequency changes. The Carrera Unified Formulation was used to derive the numerical models, as it can easily model any geometry of a structure using 1D finite elements.

Across all cases, the dynamic response of compressed Kagome metamaterials appears governed more by architecture and joint stiffness than by load level alone. In the baseline 2D lattice, the first mode softens to buckling and then hardens with clear reshaping; out-of-plane low-order modes show modest shape changes with little spectral drift, while selected higher modes undergo sizable frequency drops without identity swaps, driven by stress-stiffening relief. A small imperfection (1.5° pre-rotation) shifts the instability threshold and converts crossings into veering between the first two modes, while largely suppressing modal reshaping. Stiffer hinges

further stabilize the spectrum, flattening frequency-load trends and limiting shape changes, though a higher mode still exhibits the largest reduction (34.7%) with nearly invariant shape.

Finally, the results indicate that 3D Kagome metamaterials can deliver pre-stress-robust dynamics, limited frequency drift, minimal modal reshaping, and reduced mode interaction, making them promising candidates for load-bearing, vibration-sensitive components (e.g., precision panels, isolation layers, and space deployables) where dynamic stability under compressive service loads is critical.

The present study accounts for geometric nonlinearity, while the constitutive behavior of the base materials is assumed to be linear elastic. This modelling choice allows the role of large rotations, compressive preload, and geometry-induced tangent stiffness variations on the modal response to be isolated. However, in practical applications involving soft polymers, additively manufactured materials, or metallic lattices approaching yielding, material nonlinearity may significantly affect the effective stiffness, damping, frequency evolution, and modal transitions. The inclusion of elastoplastic, hyperelastic, or viscoelastic constitutive models therefore represents an important extension of the present work and will be addressed in future studies.

The Kagome architecture may be qualitatively interpreted as an assembly of relatively compliant hinge-like regions connecting stiffer triangular units. However, in the present configurations, the triangular units are not independent resonators attached to a surrounding host lattice. They are part of a continuous load-bearing mechanism. Therefore, the frequency-load trends observed in this work are mainly governed by preload-induced tangent stiffness variations, large rotations, and modal interaction, rather than by classical local-resonance mechanisms. Localized modal patterns may still appear in selected frequency ranges, especially near hinge regions, but a rigorous identification of local-resonance band gaps would require dedicated Bloch-Floquet and transmission analyses. This aspect is therefore identified as a natural extension of the present study.

CRediT authorship contribution statement

R. Augello: Writing – review & editing, Writing – original draft, Validation, Methodology, Formal analysis, Data curation, Conceptualization; **E. Carrera:** Writing – review & editing, Writing – original draft, Validation, Supervision, Software, Resources, Methodology, Investigation, Formal analysis, Data curation; **W.Q. Chen:** Writing – review & editing, Supervision, Methodology, Funding acquisition, Formal analysis, Data curation, Conceptualization; **B. Wu:** Writing – review & editing, Supervision, Investigation, Formal analysis, Data curation, Conceptualization; **Y.Z. Wang:** Writing – review & editing, Investigation, Funding acquisition, Formal analysis, Data curation, Conceptualization.

Declaration of competing interest

The authors declare that they have no known competing financial interests or personal relationships that could have appeared to influence the work reported in this paper.

Acknowledgement

The work was supported by the National Natural Science Foundation of China (Nos. W2511009, 12402107, 12192210 and 12192211, and U24A2005) and the 111 Project (No. B21034). This work was also partly supported by the specialized research projects of Huanjiang Laboratory, Zhuji, Zhejiang Province.

Data availability

No data was used for the research described in the article.

References

[1] B. Florijn, C. Coulais, M. van Hecke, Programmable mechanical metamaterials, Phys. Rev. Lett. 113 (17) (2014) 175503.
[2] A. Rafsanjani, A. Akbarzadeh, D. Pasini, Snapping mechanical metamaterials under tension, arXiv preprint arXiv:1612.05987 (2016).
[3] A. Rafsanjani, D. Pasini, Bistable auxetic mechanical metamaterials inspired by ancient geometric motifs, Extreme Mech. Lett. 9 (2016) 291–296.
[4] B. Haghpanah, L. Salari-Sharif, P. Pourrajab, J. Hopkins, L. Valdevit, Multistable shape-reconfigurable architected materials, Adv. Mater. 28 (36) (2016) 7915–7920.
[5] K. Che, C. Yuan, J. Wu, H. Jerry Qi, J. Meaud, Three-dimensional-printed multistable mechanical metamaterials with a deterministic deformation sequence, J. Appl. Mech. 84 (1) (2017) 011004.
[6] M. Kadic, T. Bückmann, N. Stenger, M. Thiel, M. Wegener, On the practicability of pentamode mechanical metamaterials, Appl. Phys. Lett. 100 (19) (2012).
[7] C. Zhao, Multi-plateau auxetic metamaterials with intra-and inter-cellular gradients for energy absorption, Aerotec. Missili Spaz. 105 (1) (2026) 3–11.
[8] D. Micheli, R. Pastore, A. Delfini, M. Albano, M. Marchetti, Space carbon-carbon thermal protection system electromagnetic characterization in reverberation chamber, Aerotec. Missili Spaz. 95 (2) (2016) 92–98.
[9] N. Wicks, S.D. Guest, Single member actuation in large repetitive truss structures, Int. J. Solids Struct. 41 (3–4) (2004) 965–978.
[10] S. Hyun, S. Torquato, Optimal and manufacturable two-dimensional, Kagome-like cellular solids, J. Mater. Res. 17 (1) (2002) 137–144.
[11] A.-J. Wang, D.L. McDowell, In-plane stiffness and yield strength of periodic metal honeycombs, J. Eng. Mater. Technol. 126 (2) (2004) 137–156.
[12] S.D. Guest, J.W. Hutchinson, On the determinacy of repetitive structures, J. Mech. Phys. Solids 51 (3) (2003) 383–391.
[13] K. Bertoldi, P.M. Reis, S. Willshaw, T. Mullin, Negative Poisson's ratio behavior induced by an elastic instability, Adv. Mater. 22 (3) (2010) 361–366.
[14] T.A.M. Hewage, K.L. Alderson, A. Alderson, F. Scarpa, Double-negative mechanical metamaterials displaying simultaneous negative stiffness and negative Poisson's ratio properties, Adv. Mater. 28 (46) (2016) 10323–10332.
[15] L. Ai, X.-L. Gao, Metamaterials with negative poisson's ratio and non-positive thermal expansion, Compos. Struct. 162 (2017) 70–84.
[16] J. Li, R. Bao, W. Chen, Exploring static responses, mode transitions, and feasible tunability of Kagome-based flexible mechanical metamaterials, J. Mech. Phys. Solids 186 (2024) 105599.

[17] Z.-J. Wu, F.-M. Li, C. Zhang, Vibration band-gap properties of three-dimensional Kagome lattices using the spectral element method, J. Sound Vib. 341 (2015) 162–173.
[18] H. Nassar, H. Chen, G. Huang, Microtwist elasticity: a continuum approach to zero modes and topological polarization in Kagome lattices, J. Mech. Phys. Solids 144 (2020) 104107.
[19] X. Li, R.V. Kohn, Some results on the guest–Hutchinson modes and periodic mechanisms of the Kagome lattice metamaterial, J. Mech. Phys. Solids 178 (2023) 105311.
[20] X. An, X. Yuan, H. Fan, Meta-Kagome lattice structures for broadband vibration isolation, Eng. Struct. 277 (2023) 115403.
[21] X. An, G. Sun, X. Yuan, Y. Tian, X. Hou, H. Fan, Design of Kagome lattice composite sandwich metastructures with high load bearing and low frequency vibration reduction properties, Compos. A Appl. Sci. Manuf. 174 (2023) 107716.
[22] M.J. Ablowitz, J.T. Cole, Topological insulators in longitudinally driven waveguides: Lieb and kagome lattices, Phys. Rev. A 99 (3) (2019) 033821.
[23] X. Fang, W. Lacarbonara, L. Cheng, Advances in nonlinear acoustic/elastic metamaterials and metastructures, Nonlinear Dyn. 113 (2025) 23787–23814.
[24] W. Jiao, H. Shu, V. Tournat, A theoretical framework for physically-realizable kagome metamaterials and its implications on dualities and topological edge modes, arXiv preprint arXiv:2410.04494 (2024).
[25] B. Deng, P. Wang, Q. He, V. Tournat, K. Bertoldi, Metamaterials with amplitude gaps for elastic solitons, Nat. Commun. 9 (1) (2018) 3410.
[26] K. Sun, A. Souslov, X. Mao, T.C. Lubensky, Surface phonons, elastic response, and conformal invariance in twisted kagome lattices, Proc. Natl. Acad. Sci. 109 (31) (2012) 12369–12374.
[27] G. Wu, Y. Cho, I.-S. Choi, D. Ge, J. Li, H.N. Han, T. Lubensky, S. Yang, Directing the deformation paths of soft metamaterials with prescribed asymmetric units, Adv. Mater. 27 (17) (2015) 2747–2752.
[28] X. Xin, C. Yang, Z. Wang, Y. Xing, C. Zeng, L. Liu, Y. Liu, J. Leng, 4D Printed mortise-tenon mechanical-electromagnetic multifunctional pixel metamaterials, Chem. Eng. J. 504 (2025) 158784.
[29] W. Zhang, J.E. Chen, D.X. Cao, L.H. Chen, Nonlinear dynamic responses of a truss core sandwich plate, Compos. Struct. 108 (2014) 367–386.
[30] Y. Wang, J. Liu, J. Li, X. Jing, M. Wiercigroch, Intrinsic mechanisms of vibrational mode jumping in sandwich panels, J. Sound Vib. 618 (2025) 119247.
[31] Fayyaz, S. Bashmal, A. Nazir, S. Khan, A. Alofi, Damping optimization and energy absorption of mechanical metamaterials for enhanced vibration control applications: a critical review, Polymers 17 (2) (2025) 237.
[32] M. Al Rifaie, H. Abdulhadi, A. Mian, Advances in mechanical metamaterials for vibration isolation: a review, Adv. Mech. Eng. 14 (3) (2022) 16878132221082872.
[33] A. Vigliotti, D. Pasini, Linear multiscale analysis and finite element validation of stretching and bending dominated lattice materials, Mech. Mater. 46 (2012) 57–68.
[34] M. Nikolić, E. Karavelić, A. Ibrahimbegovic, P. Miščević, Lattice element models and their peculiarities, Arch. Comput. Methods Eng. 25 (2018) 753–784.
[35] F. Maurin, F. Greco, W. Desmet, Isogeometric analysis for nonlinear planar pantographic lattice: discrete and continuum models, Contin. Mech. Thermodyn. 31 (2019) 1051–1064.
[36] Y. Wang, H. Xu, D. Pasini, Multiscale isogeometric topology optimization for lattice materials, Comput. Methods Appl. Mech. Eng. 316 (2017) 568–585.
[37] Y. Wang, Z. Wang, Z. Xia, L.H. Poh, Structural design optimization using isogeometric analysis: a comprehensive review, Comput. Model. Eng. Sci. 117 (3) (2018) 455–507.
[38] S. Lin, J. Cai, H. Xia, X. Ao, J. Liu, A reduced-order model based on finite element method for fast prediction of thermal performance of lattice structures, Int. Commun. Heat Mass Transf. 126 (2021) 105347.
[39] S. McBane, Y. Choi, Component-wise reduced order model lattice-type structure design, Comput. Methods Appl. Mech. Eng. 381 (2021) 113813.
[40] Y. Liu, G. Zheng, N. Letov, Y.F. Zhao, A survey of modeling and optimization methods for multi-scale heterogeneous lattice structures, J. Mech. Des. 143 (4) (2021) 040803.
[41] A.R. Damanpack, M. Bodaghi, W.H. Liao, Experimentally validated multi-scale modeling of 3D printed hyper-elastic lattices, Int. J. Non Linear Mech. 108 (2019) 87–110.
[42] H.W. Zhang, J.K. Wu, Z. Fu, Extended multiscale finite element method for elasto-plastic analysis of 2D periodic lattice truss materials, Comput. Mech. 45 (2010) 623–635.
[43] H. Chen, H. Nassar, G.L. Huang, A study of topological effects in 1D and 2D mechanical lattices, J. Mech. Phys. Solids 117 (2018) 22–36.
[44] H.C. Tankasala, V.S. Deshpande, N.A. Fleck, Tensile response of elastoplastic lattices at finite strain, J. Mech. Phys. Solids 109 (2017) 307–330.
[45] W.E.D. Nelissen, C. Ayas, C. Tekõglu, 2D Lattice material architectures for actuation, J. Mech. Phys. Solids 124 (2019) 83–101.
[46] E. Carrera, G. Giunta, M. Petrolo, Beam Structures: Classical and Advanced Theories, John Wiley & Sons, 2011.
[47] E. Carrera, M. Cinefra, M. Petrolo, E. Zappino, Finite Element Analysis of Structures Through Unified Formulation, John Wiley & Sons, 2014.
[48] M. Cinefra, A.G. de Miguel, M. Filippi, C. Houriet, A. Pagani, E. Carrera, Homogenization and free-vibration analysis of elastic metamaterial plates by carrera unified formulation finite elements, Mech. Adv. Mater. Struct. 28 (5) (2021) 476–485.
[49] R. Augello, E. Carrera, Nonlinear dynamics and band gap evolution of thin-walled metamaterial-like structures, J. Sound Vib. 578 (2024) 118329.
[50] E. Carrera, R. Augello, K. Abu Salem, Evaluation of the effects of different materials on the dynamic properties of thin-walled metamaterial structures, Mech. Adv. Mater. Struct. (2024) 1–16.
[51] M. Petrolo, R. Augello, E. Carrera, D. Scano, A. Pagani, Evaluation of transverse shear stresses in layered beams/plates/shells via stress recovery accounting for various CUF-based theories, Compos. Struct. 307 (2023) 116625.
[52] R. Augello, E. Carrera, W.Q. Chen, B. Wu, Y.Z. Wang, Nonlinear static analysis of metamaterial structures based on the Kagome lattice using beam finite elements and component-wise approach, Int. J. Solids Struct. 318 (2025) 113387.
[53] E. Carrera, M. Cinefra, M. Petrolo, E. Zappino, Finite Element Analysis of Structures through Unified Formulation, John Wiley & Sons, Chichester, West Sussex, UK., 2014.
[54] K.J. Bathe, Finite Element Procedures, Klaus-Jurgen Bathe, 2006.
[55] T.J.R. Hughes, The Finite Element Method: Linear Static and Dynamic Finite Element Analysis, Courier Corporation, 2012.
[56] A. Pagani, E. Carrera, Unified formulation of geometrically nonlinear refined beam theories, Mech. Adv. Mater. Struct. 25 (1) (2018) 15–31.
[57] M.A. Crisfield, An arc-length method including line searches and accelerations, Int. J. Numer. Methods Eng. 19 (9) (1983) 1269–1289.
[58] E. Carrera, A study on arc-length-type methods and their operation failures illustrated by a simple model, Comput. Struct. 50 (2) (1994) 217–229.
[59] G. Kerschen, S.W. Shaw, C. Touzé, O.V. Gendelman, B. Cochelin, A.F. Vakakis, Modal Analysis of Nonlinear Mechanical Systems, 555, Springer, 2014.
[60] R. Augello, E. Daneshkhah, X. Xu, E. Carrera, Efficient CUF-based method for the vibrations of thin-walled open cross-section beams under compression, J. Sound Vib. 510 (2021) 116232.